RSC Advances

PAPER

View Article Online
View Journal | View Issue

Cite this: *RSC Adv.*, 2024, **14**, 2633

Accelerated synthesis of 1,8-dioxo-octahydroxanthene and 1,8-dioxo-decahydroacridine derivatives using dendritic mesoporous nanosilica functionalized by hexamethylenetetramine: a novel nanocatalyst

Zahra Sabri,[ab] Nasrin Shadjou *[ab] and Mehdi Mahmoudian[ab]

Xanthene and acridine derivatives are interesting organic compounds that are used in different research fields like biomedicine and pharmaceutical science. However, applied catalysts for their synthesis have some limitations such as long reaction times, the need for harsh conditions and low yield. So, discovery of novel catalysts for the synthesis of xanthene and acridine derivatives is highly demanded. To overcome the limitation of previous methods on the efficient synthesis of 1,8-dioxo-octahydroxanthene and 1,8-dioxo-decahydroacridine derivatives, a green heterogeneous organic nano-catalyst (Cu@KCC-1–*n*Pr–HMTA) was synthesized by covalent attachment of hexamethylenetetramine to the cavities and channels of dendritic mesoporous nanosilica (KCC-1). The prepared nano-catalyst was identified using various spectroscopic and microscopic methods including scanning electron microscopy (SEM), Fourier transform infrared (FT-IR), X-ray energy diffraction (EDX), EDX mapping and nitrogen adsorption–desorption analysis (BET-BJH). The prepared green nano-catalyst showed a spherical and dendritic structure with a surface area of 65.699 $m^2\ g^{-1}$, average pore size of 40.78 nm and pore volume of 0.66 $cm^3\ g^{-1}$. Also, Cu@KCC-1–*n*Pr–HMTA has many chemo-active sites for the condensation reaction and was used as an efficient nano-catalyst towards one-step synthesis of 1,8-dioxo-decahydroacridine and 1,8-dioxo-octahydroxanthene derivatives from the reaction of aromatic aldehydes, dimedone, and ammonium acetate under solvent-free conditions. Short reaction times of 1 to 5 minutes for 1,8-dioxo-decahydroacridine and 30 to 55 minutes for 1,8-dioxo-octahydroxanthene derivatives, high yields and mild reaction conditions are advantages of the proposed synthetic method. It is hoped that the engineered nano-catalyst will be used for the synthesis of other organic compounds in the future.

Received 8th November 2023
Accepted 8th January 2024

DOI: 10.1039/d3ra07629f

rsc.li/rsc-advances

1. Introduction

Xanthenes are an important class of heterocyclic compounds that have shown a wide range of pharmacological properties such as antiviral,[1] anti-cancer,[2,3] antibacterial, antifungal,[4,5] antiplasmodial,[6] antinociceptive,[7] anti-inflammatory,[8] and DNA binding.[9] Due to the specific structure of xanthene, these compounds have been used in laser technology,[5,10] fluorescent materials for visualization of biomolecules,[11] cosmetics and pigments.[12]

Reaction of aldehydes with dimedone in the presence of various catalysts such as ionic liquids, silica sulfuric acid, resins, *para* dodecyl benzene sulfonic acid, sodium dodecyl sulfate, zinc oxide, acetyl chloride, zirconium, *para* toluene sulfonic acid, *etc.*, has been reported for the synthesis of xanthenes.[13–21] However, some of these methods have long reaction times, harsh conditions and undesirable yields. So, optimization of the methods for the efficient synthesis of xanthenes has been widely demanded by chemists.[22–24]

On the other hand, acridine derivatives are a nitrogen-containing heterocyclic organic compound with important biological activities[25] such as antimalarial[26] and chemotherapy of cancer.[27] 1,8-Dioxodihydroacridine derivatives can be prepared using quasi-four-component reaction between dimedone, aromatic aldehyde and amine or ammonium acetate in solvent-free thermal conditions in the presence of various catalysts.[28–37] Advanced nanomaterials play an important role as heterogeneous active catalysts for the synthesis of organic compounds because of easy access to internal surfaces and active functional groups that are located inside the cavities and channels of the them.[38]

Recently, dendritic nanoparticles with homocentric radial cavities act as a very useful catalytic substrate, which creates an open three-dimensional structure that to block active surfaces

[a]*Department of Nanotechnology, Faculty of Chemistry, Urmia University, Urmia, Iran. E-mail: n.shadjou@urmia.ac.ir; Tel: +98 44 32752741*
[b]*Institute of Nanotechnology, Urmia University, Urmia, Iran*

in these catalysts impossible and this increases the catalytic activity of these nanostructure. Polshettiwar and co-workers[39,40] reported a new nano-silica compound (KCC-1) with spherical, dendritic, fibrous and controlled morphology with novel physicochemical properties. These nanomaterials have been utilized for the synthesis of pharmaceutical compounds, photo-catalysts and superabsorbent for the removal of heavy metals, gas absorption, solar cells, self-cleaning materials, sensitive sensors, drug delivery and biomedical applications. Due to high surface area and accessible channels and pores, dendritic fibrous nanosilica (DFNS) is highly demanded as an advanced nanostructure for the technological approaches like organic synthesis. Also, the ability to loading various guest molecules, reactants, and solvents into their internal surface and create the available active catalytic centers, are the main advantages of these nanomaterials in different research areas.[40–42]

Hexamine,[43] also known as methamine and hexamethylenetetramine (HMTA) (Scheme 1), is a white and biocompatible crystalline heterocyclic organic compound that is highly soluble in water and polar organic solvents. This flammable solid has a cage-like structure and it has been used in the synthesis of some chemical compounds like plastic, pharmaceuticals and rubber additives. In addition, HMTA has free and readily available amino groups which can be easily participate in substitution reactions. Hence, the modified nanostructures with this functional group are chemical active compound.[44]

Due to the importance of this functional group, Noori *et al.*,[45] investigated the heterogeneous catalytic properties of hexamethylenetetramine functionalized magnetic silica in the *N*-benzylation of primary amines. Also, Ghorbani-Vaghei and Izadkhah[44] prepared hexamethylenetetramines functionalized magnetic silica towards efficient synthesis of pyranopyrazole derivatives with high yields and short reaction time.

Considering the importance of xanthene and acridine derivatives and the scope of their application in various fields, we decided to propose a new method for the synthesis of these compounds in the presence of non-toxic, inexpensive, high-performance, and new nano-catalyst, by one-pot reaction of aromatic aldehydes, dimedone and ammonium acetate under solvent-free conditions. Dendritic nanoparticles have fibrous structure with three-dimensional radial channels which lead to the efficient synthesis of pharmaceutically important compounds. So, based on the openness of nanochannels, presence of accessible interior spaces and high volume of cavities, advanced nanomaterials are interesting for the chemists. Hence, in this research, hexamethylenetetramines along with copper ions were attached to the walls and channels of KCC-1 and its catalytic properties was studied in the synthesis of 1,8-dioxo-octahydroxanthene and 1,8-dioxo-decahydroacridine derivatives. The structure of functionalized catalyst (Cu@KCC-1–*n*Pr–HMTA) is shown in Scheme 2.

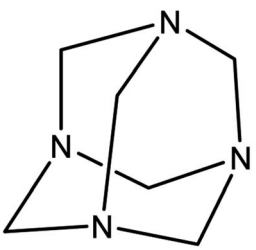

Scheme 1 Hexamethylenetetramine structure.

2. Experimental

2.1. Materials and reagents

Cetyltrimethylammonium bromide (CTAB), HMTA, ammonium acetate, aromatic aldehydes, dimedone, and cyclohexane were purchased from Merck, Germany. CTAB was used as surfactant during the synthesis of KCC-1. Tetraethyl orthosilicate (TEOS) and (3-chloropropyl)triethoxysilane were bought from Sigma-Aldrich. Also, DMF, toluene, and hexanol were purchased from Sigma-Aldrich. Deionized water was produced in laboratory. No further purification was performed on materials and reagents and they were used as-purchased.

2.2. Instruments

Philip Harris C4954718 was used to melting point measurement. Fourier transform infrared (FT-IR), spectras were obtained by Thermo-Nicolet Nexus 670 instrument. Thin layer chromatography (TLC) on Merck's silica plates were used to the monitoring of the reaction progress. The Field Emission Scanning Electron Microscopy (FE-SEM) images and Energy Dispersive X-ray (EDX) were recorded with FEG-SEM MIRA3 TESCAN, Czech Republic at 1000 kV. Brunauer–Emmett–Teller (BET) was recorded by Micromeritics NOVA 2000 (Florida, USA) apparatus at 77 K using nitrogen as the adsorption gas.

2.3. Synthesis process KCC-1

In this study, KCC-1 (bare dendritic fibrous nano-silica) was synthesized according to our previous report.[46] For this purpose, CTAB was dissolved in 10 ml of distilled water and then 0.6 g of urea was added to this solution at room temperature and the mixture was stirred by stirrer for 3 hours to dissolve the whole CTAB. In the next step, 2.3 g of TEOS as a precursor of KCC-1, 80 ml cyclohexane and 1.3 ml hexanol added to the above-mentioned solution. The mixed solution was placed at room temperature for 80 minutes under sonication, and then it was refluxed at 120 °C. After this step, the mixture was cooled to room temperature and KCC-1 was collected as bare DFNS. The nano-silica was washed three times with distilled water and twice with acetone which is necessary for its purification. The product was dried at room temperature. Finally, to remove the template, the KCC-1 was calcined in 550 °C/6 h. It is important to point out that CTAB was used as a template in the KCC-1 synthesis process by the formation of reverse micelle and urea is used for hydrolysis and condensation of orthosilicate precursor. Fig. 1 shows the synthesis procedure of KCC-1.

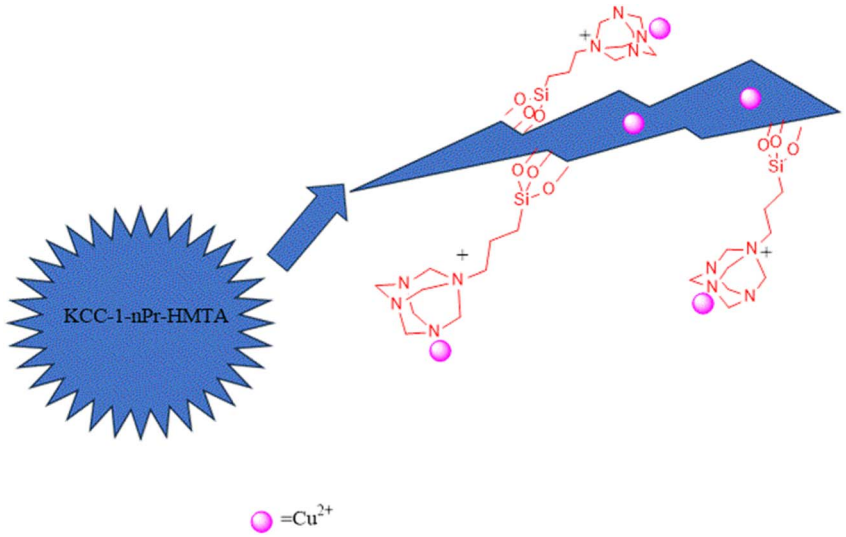

Scheme 2 Structure of functionalized catalyst (Cu@KCC-1–*n*Pr–HMTA).

2.4. Functionalization of KCC-1 with *n*-propyl chloride functional group

In this process, 0.02 g of KCC-1 was dispersed in 1.2 ml toluene and was exposed to ultrasound for 30 min. In the next step, 30 μl of 3-chloropropyltriethoxysilane was added to the solution and refluxed at 110 °C for 20 hours. Then, the modified KCC-1 was separated by centrifuge. It was washed with toluene several times and finally dried at 30 °C for 21 hours.

2.5. Functionalization of KCC-1–*n*Pr–Cl with HMTA

At first, 0.1 g of KCC-1–*n*Pr–Cl were added to the 5.2 ml of chloroform and then, HMTA was added to 2.1 ml chloroform and completely dissolved. Then, the mixture was refluxed for 5 hours. Finally, the resulting precipitate was separated by centrifuge and washed several times with distilled water and chloroform toward its purification. The desired sediment was dried at 60 °C in oven.

2.6. Doping of copper ions into the structure of KCC-1–*n*Pr–HMTA

In the process of copper-doping on the structure of KCC-1–*n*Pr–HMTA, the 5 g of the prepared nano-catalyst was added to the 1 M of copper sulfate solution with a volume of 25 ml (1 M in deionized water) and stirred for 15 h at 60 °C. Then, the obtained uniform mixture was filtered by centrifuge and the resulting sediment was dried in vacuum condition at room temperature. Finally, the blue powder was obtained as final

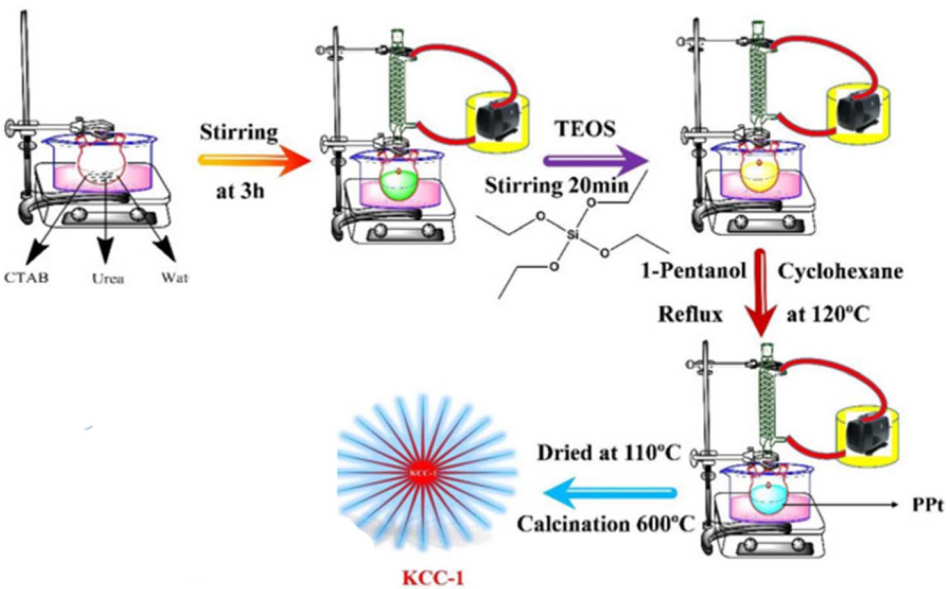

Fig. 1 Synthesis procedure of KCC-1.

nano-catalyst. Scheme 3 shows the schematic procedure of Cu@KCC-1–*n*Pr–HMTA.

2.7. General procedure of 1,8-dioxo-octahydroxanthene and 1,8-dioxo-decahydroacridine derivatives

The designed nano-catalyst Cu@KCC-1–*n*Pr–HMTA (0.02 g) was applied for the synthesis of 1,8-dioxo-octahydroxanthene and 1,8-dioxo-decahydroacridine derivatives from the reaction of aromatic aldehydes (1 mmol), dimedone and ammonium acetate (1 mmol) under solvent free conditions at 120 °C. Also, reaction process was explored by TLC (ethyl acetate/diethyl ether 1 : 2). After completion of the reaction, hot ethanol was added to the reaction mixture and the nano-catalyst was separated. The obtained products were collected and then recrystallized in EtOH (Scheme 4).

3. Results and discussion

3.1. Characterization of Cu@KCC-1–*n*Pr–HMTA

The morphology and chemical composition of functionalized and engineered nano-catalyst have been identified with a variety

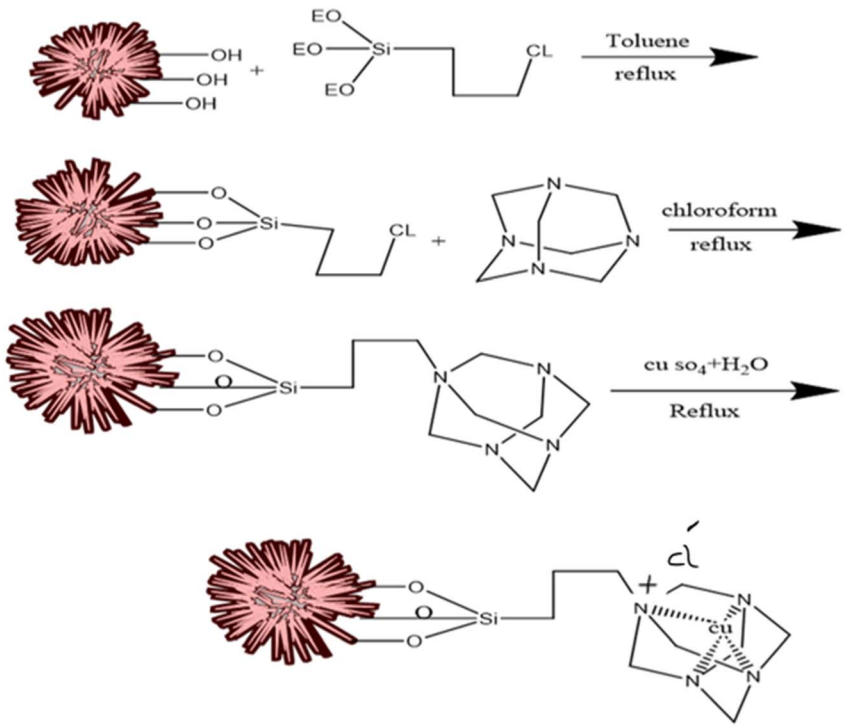

Scheme 3 Synthetic procedure of Cu@KCC-1–*n*Pr–HMTA.

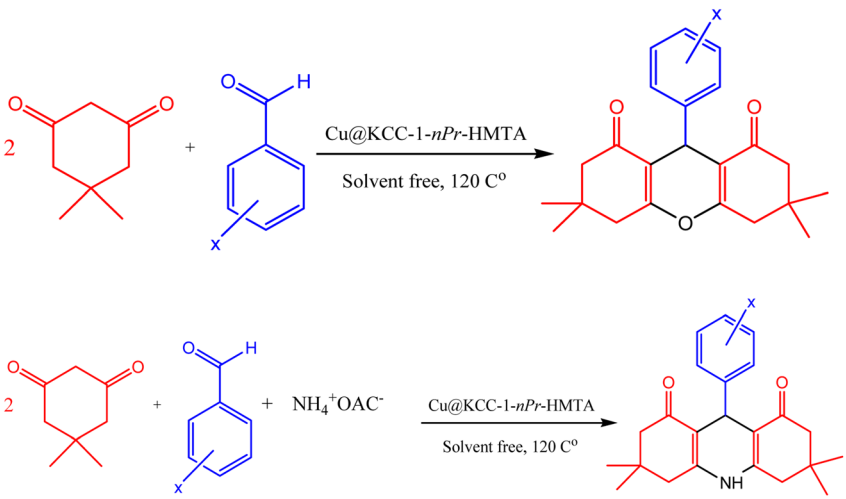

Scheme 4 Synthesis procedure of 1,8-dioxo-octahydroxanthene and 1,8-dioxo decahydroacridine derivatives in the presence of Cu@KCC-1–*n*Pr–HMTA.

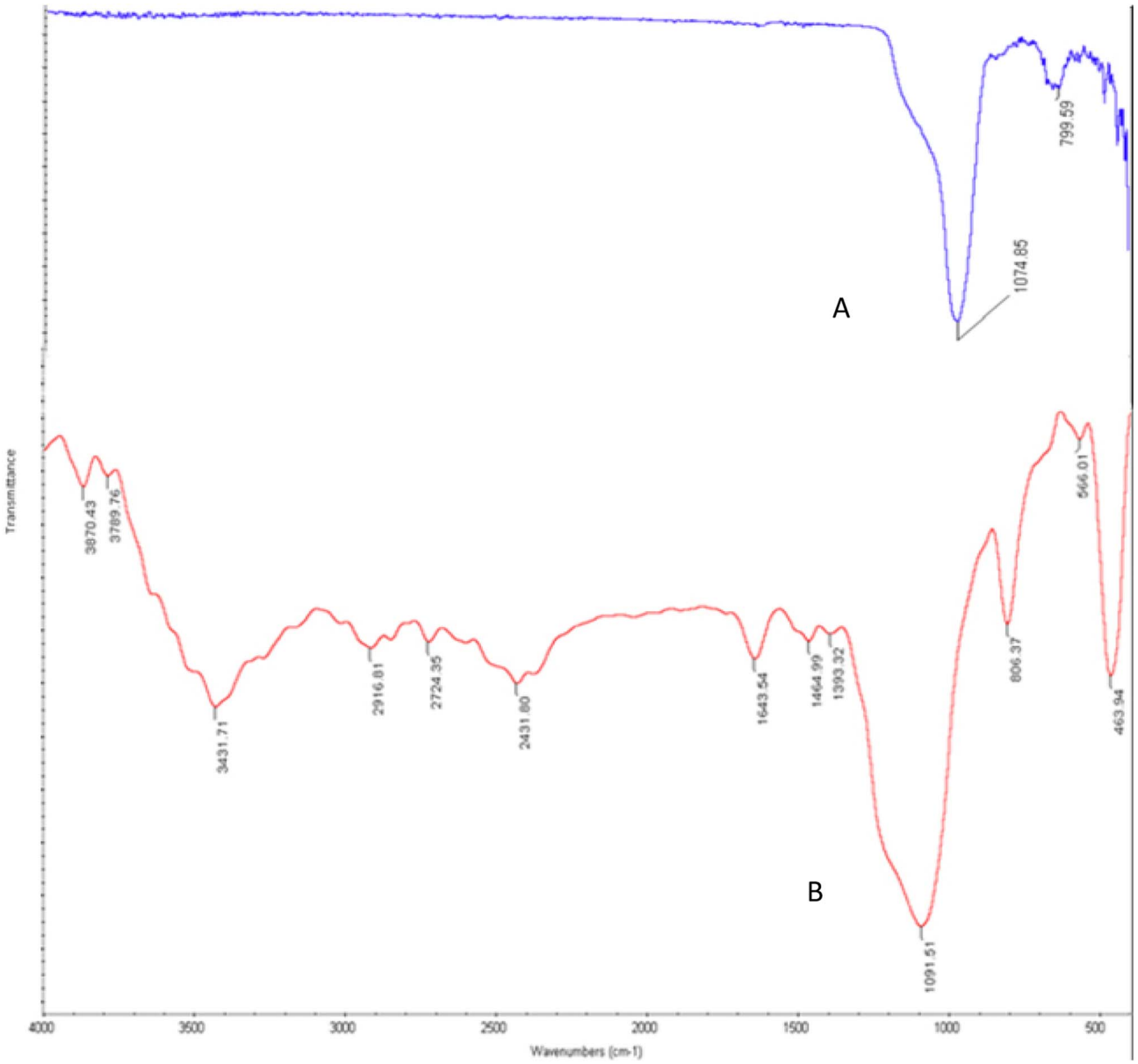

Fig. 2 FT-IR spectra of KCC-1 (A) and KCC-1–*n*Pr–HMTA (B).

of spectroscopic and microscopic analyses including FE-SEM, FT-IR, EDX, mapping, and BET-BJH methods.

The FT-IR spectrum of KCC-1 and Cu@KCC-1–*n*Pr–HMTA are presented and compared in Fig. 2. KCC-1 has a sharp peak in 1074 cm^{-1} and 799 cm^{-1} which is related to the unsymmetric and symmetric Si–O–Si stretching, respectively (Fig. 2A).

The FT-IR spectra of KCC-1–*n*Pr–HMTA was shown in Fig. 2B. The peak in 3431 cm^{-1} is related to the OH group in KCC-1. Also, the peaks in 2916 cm^{-1}, 2724 cm^{-1} are related to the stretching vibration of aliphatic C–H in functional group which attached to the pores of KCC-1. Also, the peak in 1393 cm^{-1} is related to C–N bonds.

Elemental analysis of KCC-1–*n*Pr–HMTA and Cu@KCC-1–*n*Pr–HMTA was evaluated using EDX method which is shown in Fig. 3. These elemental analyses confirm the presence of N, C, Si, O, and Cu and confirmed the functionalization of KCC-1 with hexamethylenetetramine functional group and successful loading of copper cation on the structure of prepared nano-catalyst.

Also, mapping images of KCC-1–*n*Pr–HMTA confirmed all of the obtained results by EDX method. As shown in Fig. 4, the scattering elements in the functionalized KCC-1 is including carbon, nitrogen, silicon and oxygen which shows successful functionalization of the KCC-1–*n*Pr–Cl with HMTA.

Using FE-SEM analysis, the morphology and surface properties of prepared nano-catalyst was surveyed. The spherical KCC-1–*n*Pr–HMTA has fibrous and wrinkled structure (Fig. 5). Also, a relatively balanced distribution of size can be seen in synthesized nanoparticles.

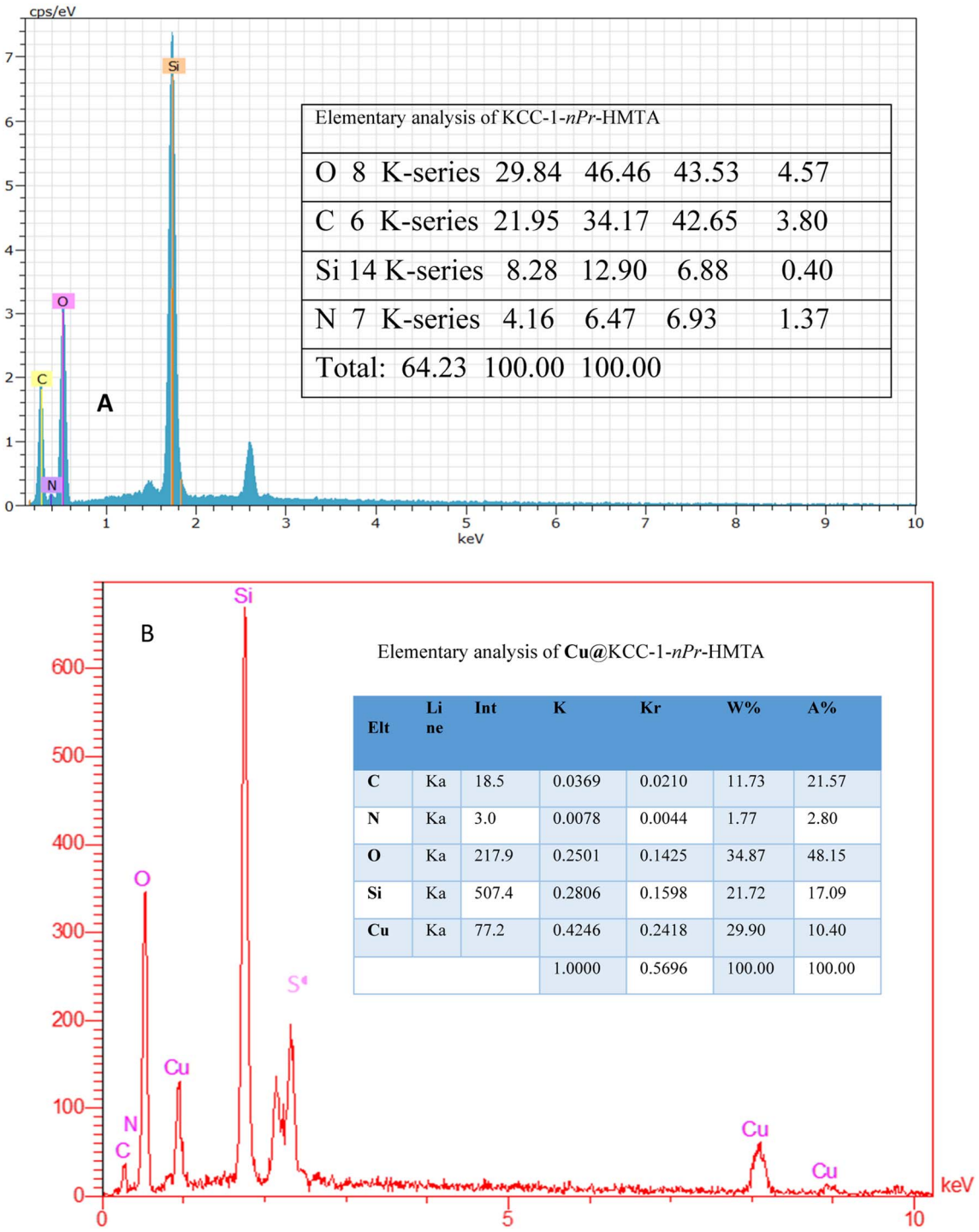

Fig. 3 EDS spectra of (A) KCC-1–*n*Pr–HMTA and (B) Cu@KCC-1–*n*Pr–HMTA.

Also, the FE-SEM images of Cu@KCC-1–*n*Pr–HMTA has been shown in Fig. 6. The spherical, fibrous and dendritic morphology of functionalized KCC-1 are obvious in all of images that recorded in different magnifications.

The results of nitrogen adsorption–desorption analysis of KCC1–*n*Pr–HMTA were indicated in Fig. 7 and surface area and pore volume of this catalyst was compared with KCC-1 and KCC-1–*n*Pr–Cl in Table 1 which shows a significant decrease in surface area and pore volume of Cu@KCC-1–*n*Pr–HMTA than KCC-1 and KCC-1–*n*Pr–Cl. So, it is confirmed the successful functionalization of KCC-1 by HMTA. The reason for the increase in the mean size of the channels can be related to the filling of channels from the central part of the KCC-1 spheres. They are pulled out of the center where the average size of the cavities is increased by functionalization. Also, according to Fig. 7, it's obvious that

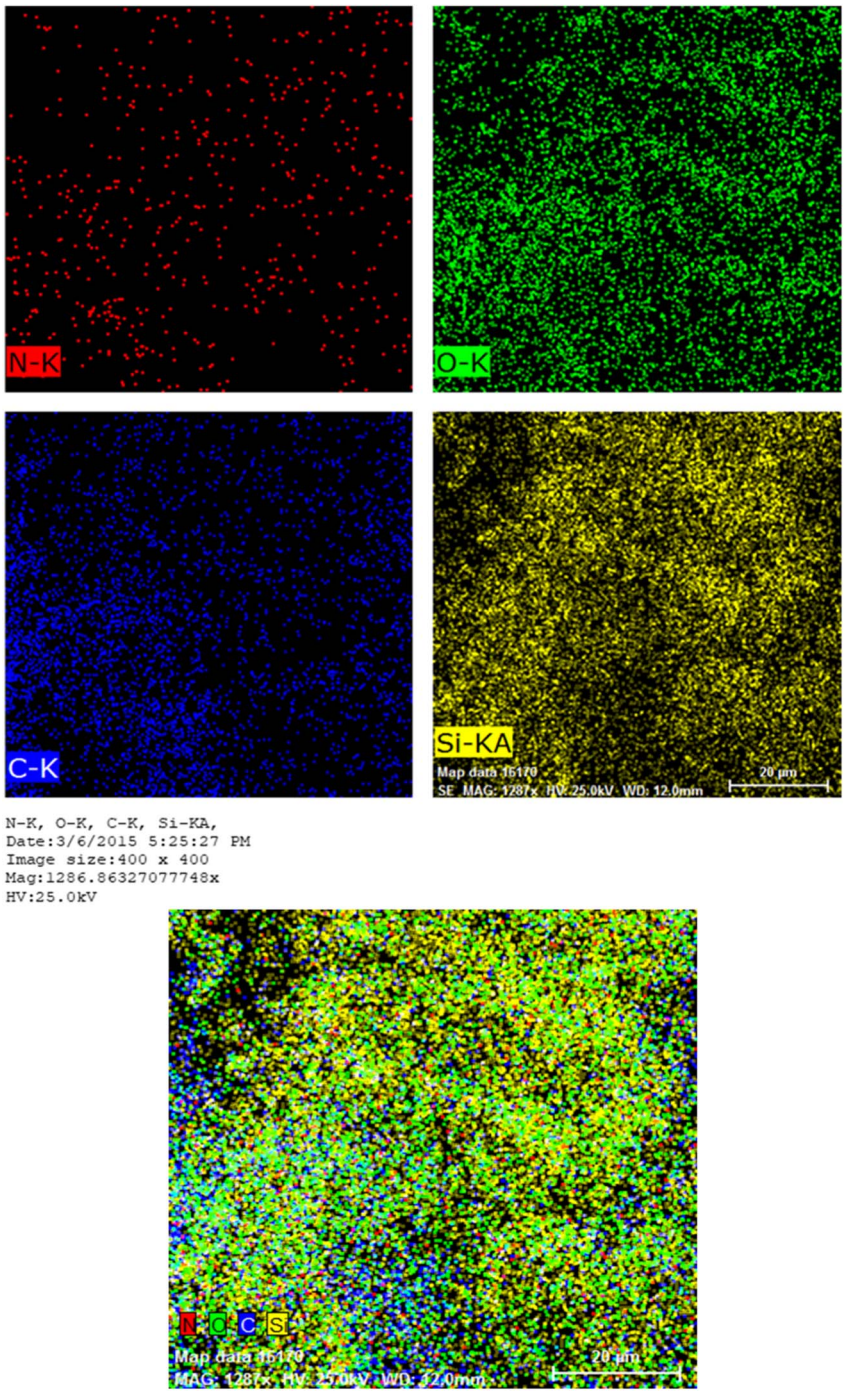

Fig. 4 Mapping images of KCC-1–*n*Pr–HMTA.

KCC1–*n*Pr–HMTA is a mesoporous nano-silica with dendritic structure.

After characterization and confirm the successful synthesis of Cu@KCC-1–*n*Pr–HMTA, its application as nano-catalyst for the efficient synthesis of 1,8-dioxo-octahydroxanthene and 1,8-dioxo-decahydroacridine derivatives were surveyed. For this purpose, the reaction of dimedone (2 mmol) and 4-chlorobenzaldehyde (1 mmol) was explored in the presence of KCC-1–*n*Pr–HMTA (0.02 g) in ethanol (5 ml) as solvent. Also, the reaction process was investigated using TLC. The reaction was completed within 25 minutes. But the results of melting point and FT-IR analysis of the product shown that the production of the reaction is a tetraketone (2,2′-((4-chlorophenyl)methylene) bis(3-hydroxy-5,5-dimethylcyclohex-2-enone)) (Scheme 5).

FT-IR spectra of prepared tetraketone is shown in the Fig. 8. The presence of broad peak in 3447 cm^{-1} corresponds to the OH functional group confirms the formation of tetraketone product in this reaction. Also, the peak appeared in the

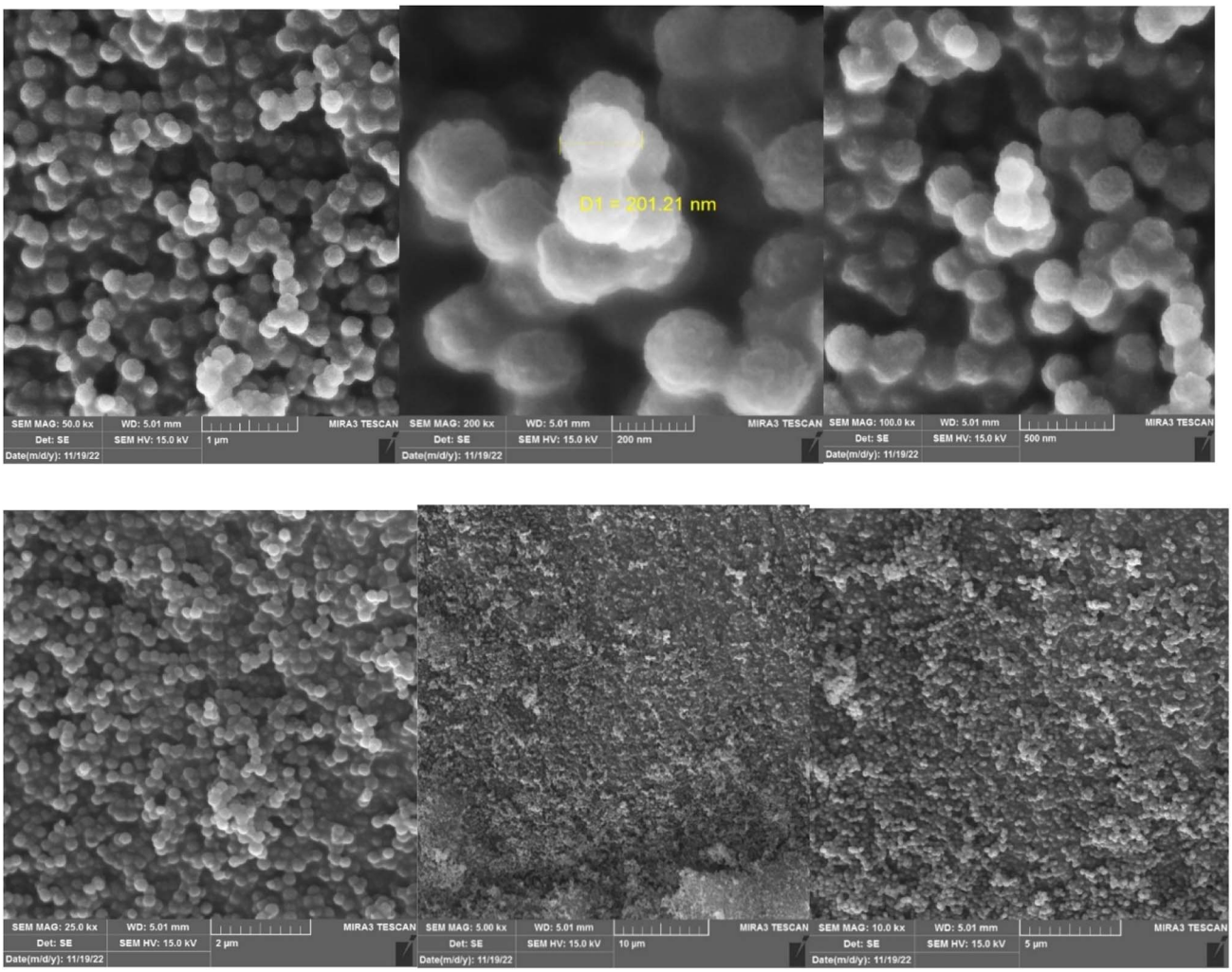

Fig. 5 FE-SEM images of KCC-1–*n*Pr–HMTA in different magnifications.

2957 cm^{-1} region is related to the stretching vibration of C–H and the peak in the 1489 cm^{-1} region is related to stretching vibration of C=C. In addition, the peak observed in the 2871 cm^{-1} region is related to the stretching vibration of aliphatic C–H. Importantly, the peak in the 1596 cm^{-1} region corresponds to the stretching vibration of C=O and the peak in the 1253 cm^{-1} region indicate the stretching vibration of C–O bond that the resonance between oxygen and the double bond causes the peak absorption appear at lower frequency. Although the tetraketone was synthesized with high yield, but it is not our desired product, and the aim of our research was the synthesis of 1,8-dioxo-octahydroxanthene and 1,8-dioxo-decahydroacridine derivatives through one-pot three-component reaction of aromatic aldehydes, dimedone and ammonium acetate in the presence of designed nano-catalyst.

In this section, one-pot three-component reaction of dimedone (2 mmol) and 4-chlorobenzaldehyde (1 mmol) was investigated in the presence of nano-catalyst (KCC-1–*n*Pr–HMTA), under solvent free condition and 120 °C. The reaction completed in 35 minutes with 98% efficiency.

Due to the FT-IR spectra of a sample a peak appeared in 2956 cm^{-1} is related to the C–H stretching vibration of C–H groups and the peaks in the range before 2956 cm^{-1} corresponds to the stretching vibration of aliphatic C–H groups (Fig. 9). Also, a peak appearing in 1578 cm^{-1} and 1490 cm^{-1} are related to the stretching vibration of C=C and the peak appeared in 1604 cm^{-1} is corresponds to the stretching vibration of C=O functional group. In addition, the peak located in the 1245 cm^{-1} indicate the stretching vibration of C–O bond, which the resonance between oxygen and double bond caused to be appeared at lower frequency. Finally, the lack of broad peak of hydroxy functional group in the region 3447 cm^{-1} confirms the synthesis of 9-(4-chlorophenyl)-3,3,6,6-tetramethyl-3,4,5,6,7,9-hexahydro-1*H*-xanthene-1,8(2*H*)-dione as product in this reaction.

The important point in this study is the effective role of copper cation as an active center in catalytic activity. At first, in order to optimization of the reaction and investigate the role of basic functional group (HMTA) in the reaction process, different types of unfunctionalized substrate (KCC-1), chloropropyl functionalized KCC-1 (KCC-1–*n*Pr–Cl) and HMTA

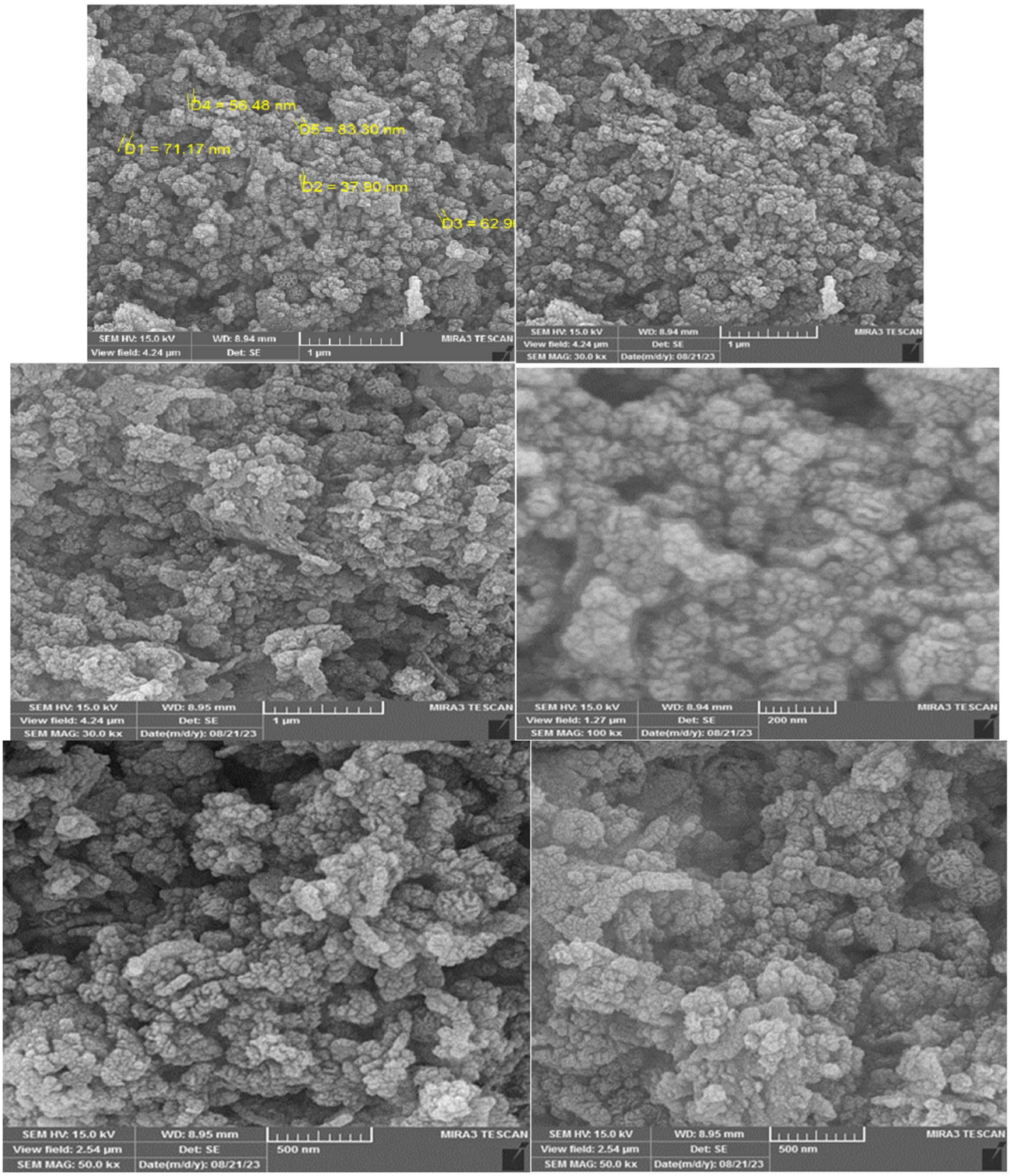

Fig. 6 FE-SEM images of Cu@KCC-1–*n*Pr–HMTA different magnification.

functionalized KCC-1 (KCC-1–*n*Pr–HMTA) were also used in reaction of dimedone (2 mmol) and 4-chlorobenzaldehyde (1 mmol) under solvent-free condition at 120 °C and in the presence of 0.02 g of nano-catalyst. The results showed that, in the presence of KCC-1 and KCC-1–*n*Pr–Cl the reaction time was long (130 min) and the product with low yield (10%) was obtained (entries 1 and 2, Table 2). But in the presence of 0.02 g of the designed nano-catalyst (KCC-1–*n*Pr–HMTA), the yield of the product was 90% and reaction time was reduced to 60 min (entry 3, Table 2). After loading the copper ions in the channels

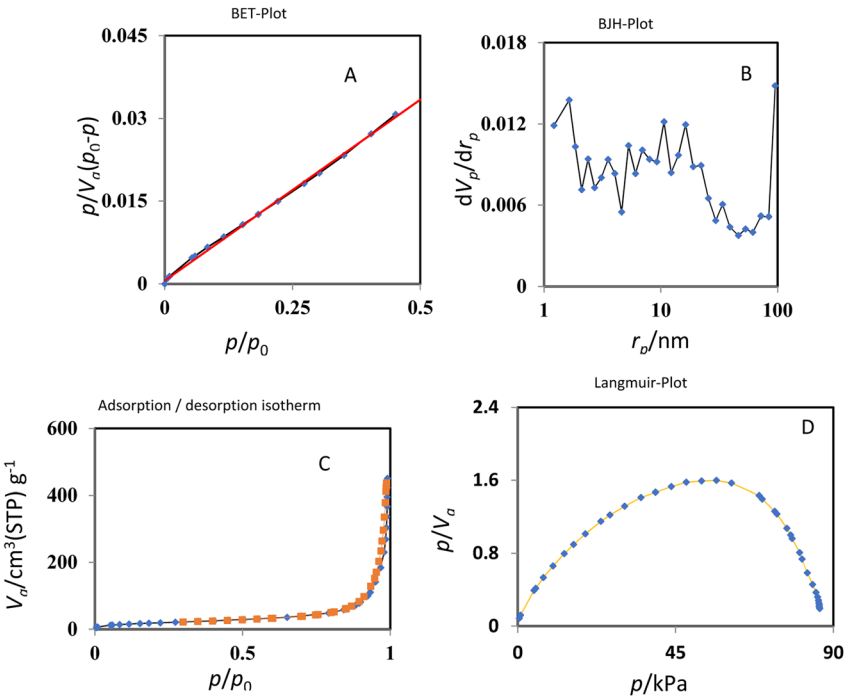

Fig. 7 BET (A), BJH (B), absorption and desorption isotherms (C), and Langmuir-plot (D) of KCC1–*n*Pr–HMTA.

Table 1 The surface area (m^2 g^{-1}), mean pore size (nm) and pore volume (cm^3 g^{-1}) of KCC-1, KCC-1–*n*Pr–Cl, and KCC1–*n*Pr–HMTA

Sample	Surface area (m^2 g^{-1})	Average pore size (nm)	Pore volume (cm^3 g^{-1})
KCC-1	617	9.9	1.5
KCC-1–*n*Pr–Cl	386	12.4	1.1
KCC-1–*n*Pr–HMTA	65.699	40.781	0.66

and pores of the catalyst (KCC-1–*n*Pr–HMTA) and applying it in the synthesis of 1,8-dioxo-octahydroxanthene derivatives, the product was obtained in the lowest time (30 min) with the highest yield (98%) under solvent-free conditions (entry 4, Table 2). According to the results indicated in Table 2, the use of copper cation plays a significant role in increasing the yield of the reaction and shortens the reaction time. Therefore, Cu@KCC-1–*n*Pr–HMTA (0.02 g) was selected as the optimal

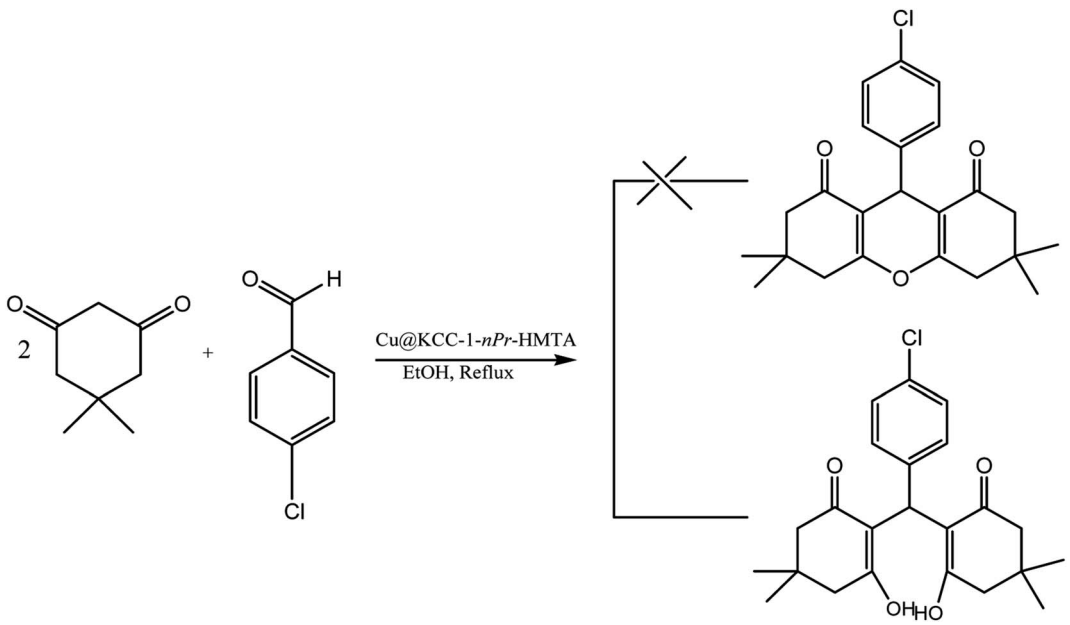

Scheme 5 Synthesis of tetraketone in the presence of ethanol as solvent and under reflux conditions.

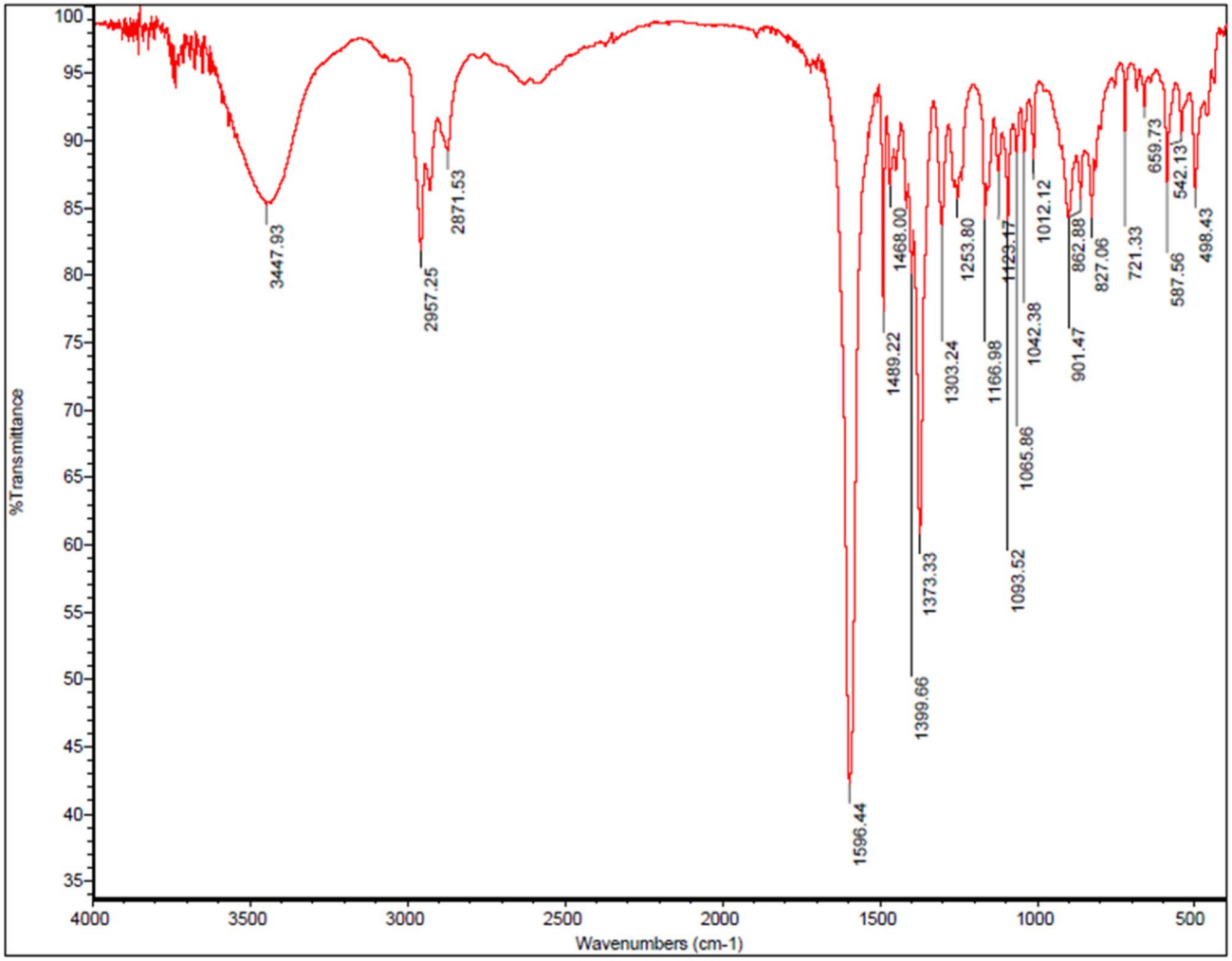

Fig. 8 FT-IR spectra of tetraketone (2,2′-((4-chlorophenyl)methylene)bis(3-hydroxy-5,5-dimethylcyclohex-2-enone)).

catalyst in the reaction of 1,8-dioxo-octahydroxanthene derivatives.

Also, different solvents such as ethanol, water/ethanol and dimethylformamide were used to investigate their effect in the time and yield of the reaction. According to the obtained results, (entry 1, Table 3), when the reaction of dimedone (2 mmol) and 4-chlorobenzaldehyde (1 mmol) was done in the presence of Cu@KCC-1–*n*Pr–HMTA (0.02 g) and ethanol as a solvent under reflux conditions, the yield of reaction product was about 80% in 25 minutes. However, after crystallization of the obtained product, the formation of tetraketone was confirmed by IR spectra and melting point.

In the next step, the yield of the reaction between dimedone (2 mmol) and 4-chlorobenzaldehyde (1 mmol) was negligible in the presence of Cu@KCC-1–*n*Pr–HMTA (0.02 g) as catalyst and water/ethanol (1 : 1) as solvent under reflux conditions in 90 minutes (entry 2, Table 3). Continuously, when DMF was used as solvent at 70 °C (entry 3, Table 3), the product of the reaction was obtained in 70 minutes with 60% yield. In the next step, the same reaction was investigated in DMF as solvent in the presence of Cu@KCC-1–*n*Pr–HMTA as catalyst at 120 °C (entry 4, Table 3). The results showed that the reaction product was obtained in 40 min with 60% efficiency. In the next step, the same reaction was obtained in the presence of 0.02 g of KCC-1–*n*Pr–HMTA as catalyst under solvent-free conditions at 120 °C (entry 5, Table 3). The results of TLC showed that the product was obtained in 60 min with 90% yield. After crystallization of obtained product in ethanol, the 1,8-dioxo-octahydroxanthene derivatives were confirmed by FT-IR spectroscopy and determination of melting point.

In order to achieve the optimum catalytic amount, the same experiment was carried out with the same conditions and the same reagents for xanthene synthesis in the presence of KCC-1–*n*Pr–HMTA catalyst (entry 6, Table 3). The reaction was completed under solvent-free conditions and at 120 °C in 90 min with 90% efficiency and after crystallization of xanthene, the product was detected by FT-IR spectroscopy and its melting point was determined. Then, for the reaction of dimedone (2 mmol) and 4-chlorobenzaldehyde (1 mmol) for preparation of xanthene product in the presence of (0.01 g) KCC-1–*n*Pr–HMTA, the reaction time was 90 min with 90% efficiency under solvent-free conditions and 120 °C. In the following, by loading copper

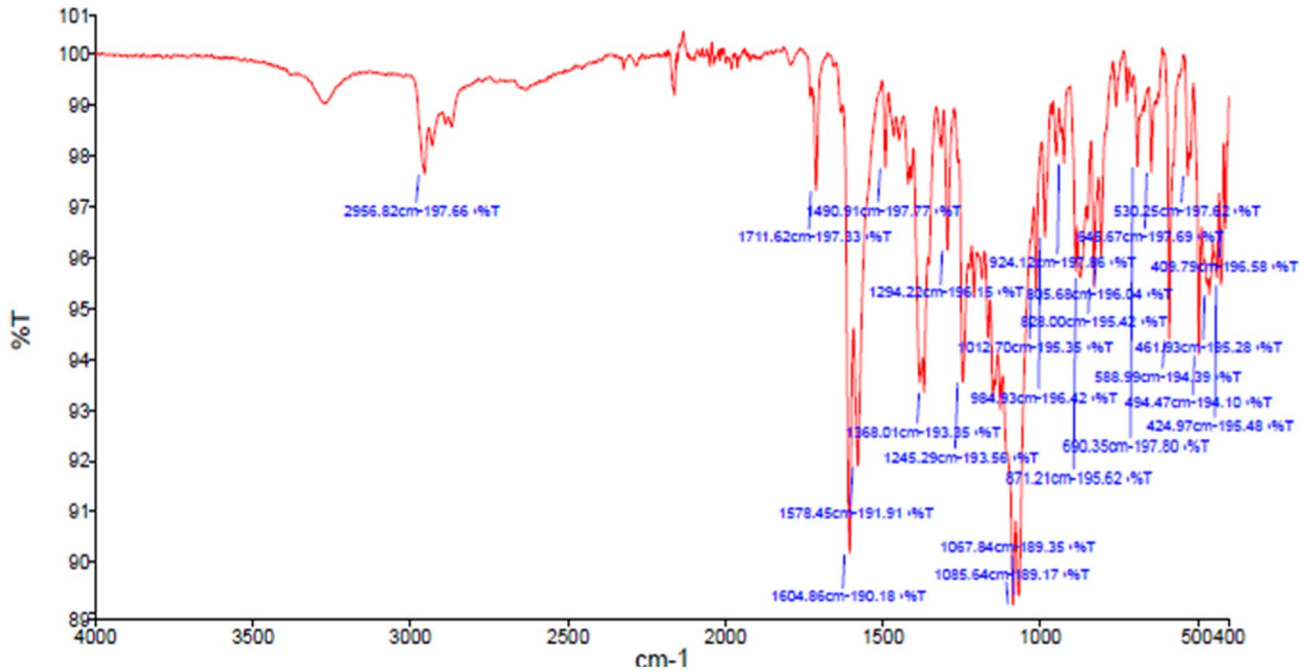

Fig. 9 FT-IR spectra of 9-(4-chlorophenyl)-3,3,6,6-tetramethyl-3,4,5,6,7,9-hexahydro-1*H*-xanthene-1,8(2*H*)-dione.

Table 2 Comparison of the time (min) and yield (%) of the 1,8-dioxo-octahydroxanthene derivatives synthesis based on various types of KCC-1

Entry	Catalyst	Temperature (°C)	Time (min)	Yield (%)
1	KCC-1 (0.02 g)	120	130	10
2	KCC-1–*n*Pr–Cl (0.02 g)	120	130	10
3	KCC-1–*n*Pr–HMTA (0.02 g)	120	60	90
4	Cu@KCC-1–*n*Pr–HMT (0.02 g)	120	30	98

Table 3 Comparison of the effect of various reaction conditions for xanthan synthesis

Entry	Catalyst	Solvent	Temperature (°C)	Time (min)	Yield (%)
1	Cu@KCC-1–*n*Pr–HMTA (0.02 g)	Ethanol	Reflux	25	80
2	Cu@KCC-1–*n*Pr–HMTA (0.02 g)	Water and ethanol	Reflux	90	—
3	Cu@KCC-1–*n*Pr–HMTA (0.02 g)	DMF (2 drops)	70	70	60
4	Cu@KCC-1–*n*Pr–HMTA (0.025 g)	DMF (2 drops)	120	40	60
5	KCC-1–*n*Pr–HMTA (0.02 g)	No solvent	120	60	90
6	KCC-1–*n*Pr–HMTA (0.01 g)	No solvent	120	90	90
7	Cu@KCC-1–*n*Pr–HMTA (0.02 g)	No solvent	120	30	98
8	No catalyst	No solvent	120	60	—

ions in the structure of designed nano-catalyst (Cu@KCC-1–*n*Pr–HMTA), the product was obtained in the shortest time (30 min) with the highest efficiency (98%) in solvent-free conditions (entry 7, Table 3). In the last step, the reaction was carried out at 120 °C under solvent-free conditions in the presence of catalyst. The reaction was completed in 60 min with negligible efficiency (entry 8, Table 3). Based on the obtained results indicated in Table 3, it can be concluded that solvent-free conditions are a green method and an appropriate option for advancing the reaction. On the other hand, costs will be reduced and we will have a green reaction that will not harm the environment. Accordingly, the above conditions play an effective role in this reaction. Therefore, 0.02 g of Cu@KCC-1–*n*Pr–HMTA catalyst and solvent-free conditions and 120 °C were selected as optimum reaction conditions.

According to the data obtained from the condensation reaction of dimedone and aromatic aldehydes using the newly synthesized nano-catalyst, 1,8-dioxo-octahydroxanthene derivatives were

Table 4 Synthesized of 1,8-dioxo-octahydroxanthene derivatives in the presence of Cu@KCC-1–*n*Pr–HMTA and solvent free condition

Entry	Products	Time (min)	Yield (%)	Melting point (reported)	Melting point (°C)	Ref.
1	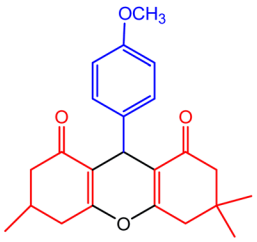	50	95	242–245	243–245	47
2	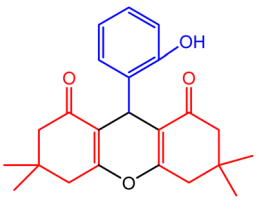	45	80	231–233	230–233	48
3	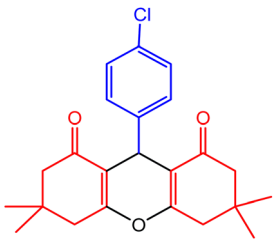	30	98	230–232	228–230	47
4	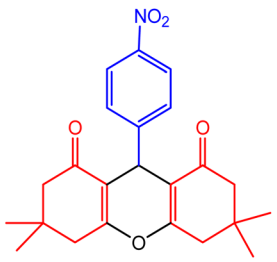	50	98	221–223	219–222	49
5	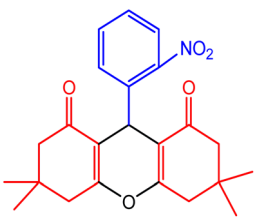	55	90	248–249	246–248	49
6	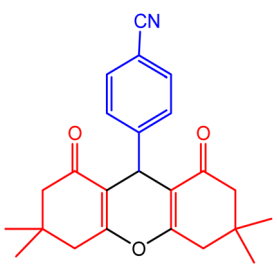	30	95	217–218	217–218	50

Table 4 (*Contd.*)

Entry	Products	Time (min)	Yield (%)	Melting point (reported)	Melting point (°C)	Ref.
7	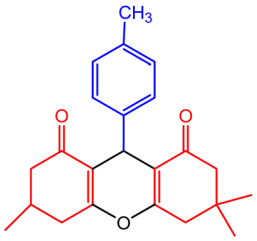	40	95	219–221	215–221	50
8	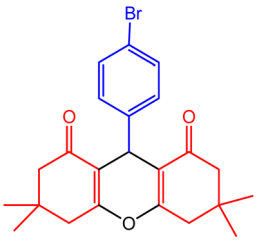	32	90	240–242	240–242	50

produced with excellent yield and in a short reaction time. The products were synthesized in solvent-free conditions and within 30 to 45 minutes without by-products (Table 4).

The Scheme 6 shows the mechanism for the synthesis of 1,8-dioxo-octahydroxanthene derivatives in the presence of Cu@KCC-1–*n*Pr–HMTA as nano-catalyst. Loading of copper

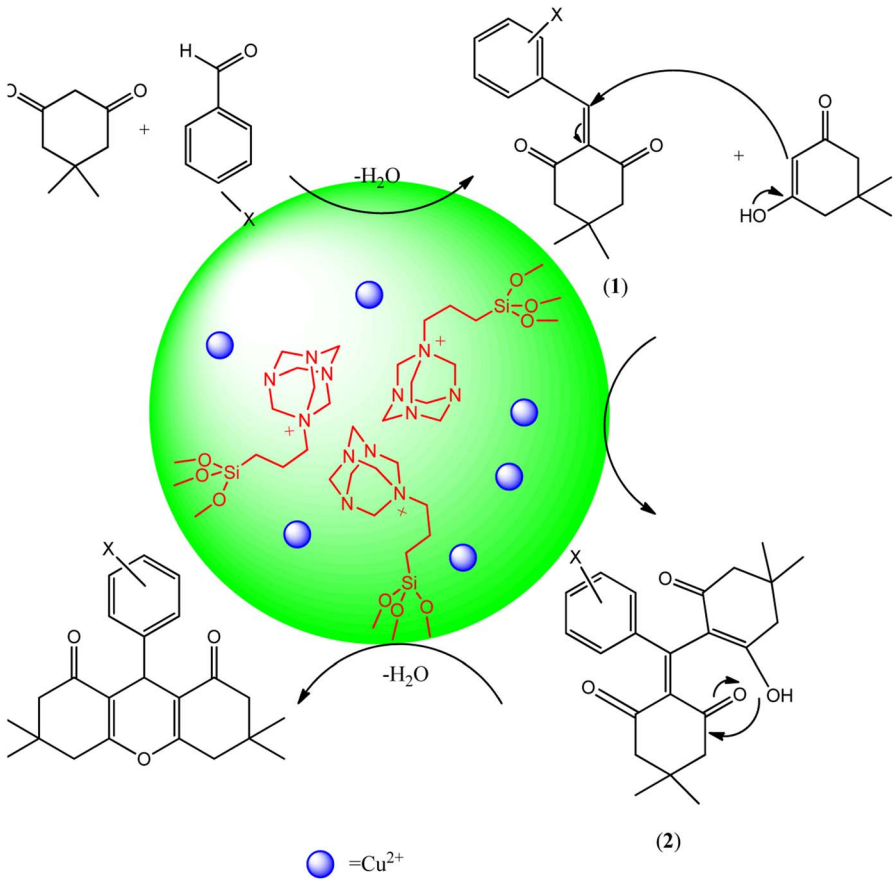

Scheme 6 Synthesis mechanism of 1,8-dioxo-octahydroxanthene derivatives in the presence of Cu@KCC-1–*n*Pr–HMTA as green nano-catalyst.

ions as a Lewis acid in the designed nano-catalyst have a significant impact on the catalytic performance. In the early stages of the reaction, reactants interact with copper ion as Lewis acid and HMTA as a basic group in the channels and pores of designed nano-catalyst. The copper ions interact with carbonyl of aromatic aldehydes and dimedone. Hence, the carbonyl groups are activated and the H-hydrogen that present in dimedone structure which becomes more acidic. It accelerates the Knoevenagel condensation between carbonyl of aromatic aldehydes and activated carbon of dimedone and led to formation of intermediate **1**. Then, through Michael's addition, the other dimedone that has the catalyst-activated carbonyl group, is attached to the intermediate **1** and finally the product was synthesized. So, the reaction efficiency is increased and the synthesis time is shortened. Similar results were obtained by previous reports.[17,51,52]

In this section, the results of synthesis of 1,8-dioxo-octahydroxanthene derivatives are compared with other synthetic methods presented in the previous reports that indicated in the Table 5. High yields (80–98%) and short reaction times (30 to 55 min) are important advantages of designed nano-catalyst. These factors facilitate the synthesis of 1,8-dioxo-octahydroxanthene derivatives and highly efficient production.

Due to the appropriate activity of the designed catalyst (Cu@KCC-1–*n*Pr–HMTA) for the one-step synthesis of 1,8-dioxo-octahydroxanthene derivatives, we decided to investigate the reaction of dimedone, aromatic aldehydes and ammonium acetate salt for the synthesis of 1,8-dioxo-decahydroacridine derivatives in the presence of designed nano-catalyst. For this purpose, the reaction of dimedone (2 mmol), 4-chlorobenzaldehyde (1 mmol) and ammonium acetate (1 mmol) was tested in the presence of 0.02 g of catalyst (Cu@KCC-1–*n*Pr–HMTA) and ethanol/water as solvent under reflux conditions. Also, the reaction process was investigated using TLC. Under these conditions, the reaction efficiency was negligible (Table 6, entry 1). Then, this reaction was tested in the presence of 0.02 g catalyst and ethanol as solvent under reflux conditions. After 120 minutes the reaction yield was 80% (Table 6, entry 2). In the following the reaction of dimedone (2 mmol), 4-chlorobenzaldehyde (1 mmol), and ammonium acetate (0.1 g) in the presence of 0.02 g catalyst, solvent-free conditions and 120 °C was investigated. The results showed that under these conditions and within 2 minutes, the reaction product was achieved with 98% of yield (Table 6, entry 3). In the last step, to compare the performance of the designed catalyst, the same reaction was investigated under solvent-free and without catalyst at 110 °C. Longer reaction time (60 minutes) and lower yield was associated with the results (Table 6, entry 4). Therefore, solvent-free conditions, temperature of 120 °C and 0.02 g of catalyst were selected as optimum conditions for the synthesis of 1,8-dioxo-decahydroacridine derivatives.

In order to synthesis of 1,8-dioxo-decahydroacridine derivatives, aldehydes with electron-donating groups such as methoxy, methyl, hydroxy and aldehydes with electron-withdrawing groups such as chloro- and nitro-groups on aromatic ring were used for the reaction. The data presented in Table 7 show that in the presence of nano-catalyst and under solvent-free conditions, 1,8-dioxo-decahydroacridine derivatives were synthesized in very short reaction times (1 to 5 minutes) with high yields without by-products.

The proposed mechanism of 1,8-dioxo-decahydroacridine synthesis in the presence of dendritic nanosilica Cu@KCC-1–*n*Pr–HMTA is shown in Scheme 7. The copper which doped in the designed nano-catalyst acts as a Lewis acid and has a significant effect on the catalyst's performance which

Table 5 Comparison of the performance of different catalysts in synthesis of the 1,8-dioxo-octahydroxanthene

Catalyst	Solvent	Temperature (°C)	Time (min)	Yield (%)	Ref.
[Bmim]HSO_4	No solvent	80	180	85	13
Boric acid	No solvent	20	120	98	53
CuO NPs	No solvent	100	14	89	54
$HClO_4$–SiO_2	No solvent	140	180	90	33
Fe_3O_4@SiO_2@KCC-1@MPTMS@Cu	No solvent	110	70	95	55
[SO_3H–pyrazine–SO_3H]Cl	No solvent	110	35	93	56
[TMXH]FeCl	No solvent	110	10	92	57
Fe–X	No solvent	90	15	95	58
Cu@KCC-1–*n*Pr–HMTA	No solvent	120	30	98	This work

Table 6 Optimization of reaction condition for the synthesis of 1,8-dioxo-decahydroacridine

Entry	Catalyst	Solvent	Temperature (°C)	Reaction time (min)	Yields%
1	Cu@KCC-1–*n*Pr–HMTA (0.02 g)	Ethanol and water	Reflux, 70	50	—
2	Cu@KCC-1–*n*Pr–HMTA (0.02 g)	Ethanol	Reflux, 70	120	80
3	Cu@KCC-1–*n*Pr–HMTA (0.02 g)	Solvent free	120	2	98
4	No catalyst[55]	Solvent free	110	60	70

Table 7 Comparison the synthesis time (min) and yield (%) of 1,8-dioxo-decahydroacridine derivatives under solvent-free conditions in the presence of Cu@KCC-1–*n*Pr–HMTA (0.02 g) as nano-catalyst

Entry	Products	Time (min)	Yields%	Melting point	Melting point (°C)	Ref.
1	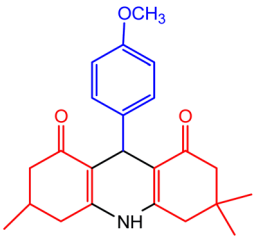	2	95	311–313	311–313	32
2	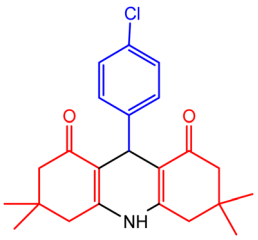	2	98	317–320	318–320	59
3	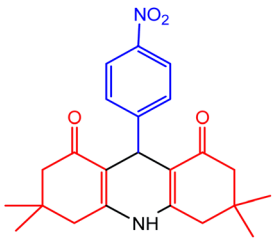	3	98	320–322	320–322	32
4	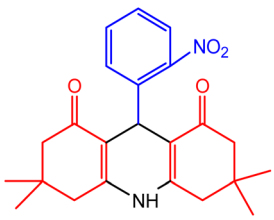	5	88	348–349	347–349	32
5	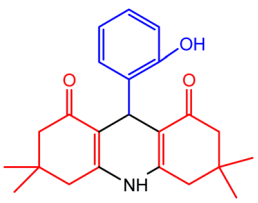	2	50>	371–373	371–373	59
6	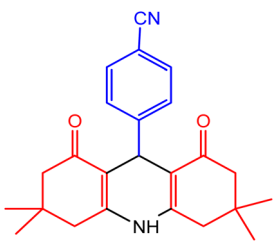	2	95	328–330	328–330	59

Table 7 (*Contd.*)

Entry	Products	Time (min)	Yields%	Melting point	Melting point (°C)	Ref.
7	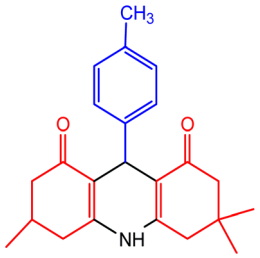	1	96	331–332	331–332	59
8	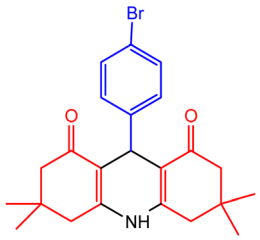	1	97	230–232	230–232	59

accelerate of the reaction kinetic. In other words, in the presence of dendritic structure of catalyst, with easier access and diffusion of reactants to the active sites (channels and pores), the intermediate can be formed inside the channels and the reaction efficiency is increased and the synthesis time is shortened. On the other hand, due to the Lewis acid properties

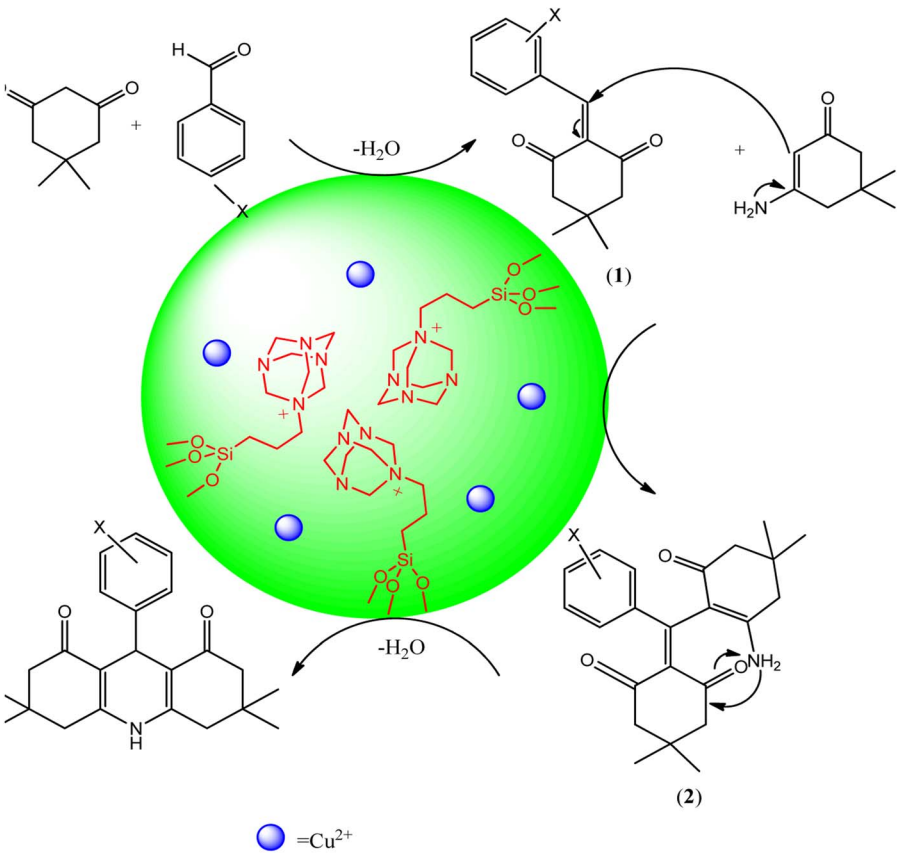

Scheme 7 Synthesis mechanism of 1,8-dioxo-decahydroacridine derivatives in the presence of designed catalyst (Cu@KCC-1–*n*Pr–HMTA).

Table 8 Comparison of the performance of different catalysts in the efficient synthesis of 1,8-dioxo-decahydroacridine

Entry	Catalyst	Solvent	Temperature (°C)	Time (min)	Yield (%)	Ref.
1	Cu@KCC-1–*n*Pr–HMTA	Solvent-free	120	2	98	This work
2	MCM-41–SO_3H	Solvent-free	110	10	95	64
3	SiO_2–Pr–SO_3H	Solvent-free	120	120	95	65
4	Na^+–MMT–[bip]-NH_2^+–H_2SO_4	Solvent-free	120	10	95	66
5	Acetic acid	Solvent-free	80	10	81	31
6	Choline chloride	Ethanol	120	180	98	67
7	KCC-1–*n*Pr–NH–Arg	Solvent-free	110	30	98	68

of copper ions and basic properties of HMTA, the condensation occurs between activated carbonyl groups, dimedone and ammonium acetate which lead to the formation of intermediate **1**. Then, by Michael addition of other dimedone to the intermediate **1** and lastly after cycloaddition reactions, the final product is formed. These results were confirmed by previous reports.[60–64]

In summary, the performance of different catalysts were investigated for the reaction of 1,8-dioxo-decahydroacridine synthesis in comparison with designed catalyst (Table 8). Solvent-free conditions, stoichiometry use of reactants, high efficiency and short reaction time (1–5 min) are important features of applied nano-catalyst in synthesis.

In summary, the advantages this catalyst (Cu@KCC-1–*n*Pr–HMTA) is its nanostructure, which by creating a very high surface area, allows the reaction to perform in a much more suitable condition than previous reports. In this method, instead of using solvents or toxic catalysts, solvent-free conditions in the presence of silica based mesoporous nano-material as a basic solid catalyst were applied which is environmentally friendly, along with easy and simple synthesis, high efficiency and very short time of reaction for the synthesis of 1,8-dioxo-decahydroacridin and 1,8-dioxo-octahydroxanthene derivatives.

4. Conclusion

In this study, Cu@KCC-1–*n*Pr–HMTA was prepared and evaluated for the efficient synthesis of 1,8-dioxo-octahydroxanthene and 1,8-dioxo-decahydroacridin derivatives. Using this green dendritic nano-catalyst, the synthesis of xanthene and acridine derivatives was done in solvent-free and non-toxic reaction conditions which do not harm living organisms and environment. Also, one-step synthesis, low amounts of catalyst, high yields and shorter reaction times and purity of the products, are other advantages of this nano-catalyst.

Conflicts of interest

There are no conflicts to declare.

Acknowledgements

We gratefully acknowledge the support of this work by Urmia University.

References

1 J. M. Jamison, K. Krabill, A. Hatwalkar, E. Jamison and C. C. Tsai, *Cell Biol. Int. Rep.*, 1990, **1**, 1075–1084.
2 G. W. Rewcastle, G. J. Atwell, L. Zhuang, B. C. Baguley and W. A. Denny, *J. Med. Chem.*, 1991, **11**, 217–222.
3 N. Mulakayala, P. V. Murthy, D. Rambabu, M. Aeluri, R. Adepu, G. R. Krishna, C. M. Reddy, K. R. Prasad, M. Chaitanya, C. S. Kumar and M. B. Rao, *Bioorg. Med. Chem. Lett.*, 2012, **6**, 2186–2191.
4 T. Gu, M. Zhang, J. Chen and H. Qiu, *Chem. Commun.*, 2015, **51**, 9825–9828.
5 A. Paiva, R. Craveiro, I. Aroso, M. Martins, R. L. Reis and A. R. C. Duarte, *ACS Sustainable Chem. Eng.*, 2014, **2**, 1063–1071.
6 A. G. B. Azebaze, M. Meyer, A. Valentin, E. L. Nguemfo, Z. T. Fomum and A. E. Nkengfack, *Chem. Pharm. Bull.*, 2006, **54**, 111–113.
7 E. F. Llama, C. Campo, M. Capo and M. Anadon, *Eur. J. Med. Chem.*, 1989, **24**, 391–396.
8 A. G. Banerjee, L. P. Kothapalli, P. A. Sharma, A. B. Thomas, R. K. Nanda, S. K. Shrivastava and V. V. Khatanglekar, *Arabian J. Chem.*, 2016, **9**, S480–S489.
9 R. Kakadiya, H. Dong, A. Kumar, D. Narsinh, X. Zhang, T. Chou, T. Lee, A. Shah and T. Su, *Bioorg. Med. Chem.*, 2010, **18**, 2285–2299.
10 M. B. Taysun, E. Sert and F. S. Atalay, *J. Chem. Eng. Data*, 2017, **62**, 1173–1181.
11 C. G. Knight and T. Stephens, *Biochem. J.*, 1989, **258**, 683–689.
12 M. A. Zolfigol, R. Ayazi-Nasrabadi, S. Baghery, V. Khakyzadeh and S. Azizian, *J. Mol. Catal. A: Chem.*, 2016, **418**, 54–67.
13 K. Niknam and M. Damya, *J. Chin. Chem. Soc.*, 2009, **56**, 659.
14 M. Salami and A. Ezabadi, *Res. Chem. Intermed.*, 2019, **45**, 3673.
15 A. N. Dadhania, K. P. Vaibhav and K. R. Dipak, *J. Saudi Chem. Soc.*, 2017, **21**, 163.
16 F. A. Darweesh, S. K. Salama, I. A. Abdelhamid and A. H. M. Elwahy, *Synth. Commun.*, 2021, **51**, 471.
17 A. M. Bhat, A. M. Naglah, S. A. Ansari, H. M. Al-Tuwajiri and A. A. Dhfyan, *Molecules*, 2021, **26**, 3667.
18 P. Mane, B. Shinde, P. Mundada, V. Gawade, B. Karale and A. Burungale, *Res. Chem. Intermed.*, 2020, **46**, 231.
19 M. Salam and A. Ezabadi, *Res. Chem. Intermed.*, 2019, **45**, 3673.

20 H. A. Bhatt, V. R. Shah and R. M. Rawal, *World Sci. News*, 2019, **118**, 100.
21 M. M. Hosseini, E. Kolvari, M. Vahidian and R. Bagheri, *J. Appl. Chem.*, 2017, **11**, 109.
22 M. Havaei, B. Karami and S. Khodabakhshi, *Curr. Chem. Lett.*, 2014, **3**, 167.
23 K. S. Kanakikodi, S. R. Churipard, A. B. Halgeri and S. P. Maradur, *Sci. Rep.*, 2020, **10**, 13103.
24 M. Akhtarkavian and Z. Rafiee, *J. Appl. Chem.*, 2020, **15**, 9.
25 R. Shan, C. Velazquez and E. E. Knaus, *J. Med. Chem.*, 2004, **47**(1), 254–261.
26 S. Girault, P. Grellier, A. Berecibar, *et al.*, *J. Med. Chem.*, 2000, **43**(14), 2646–2654.
27 W. M. Cholody, B. Horowska, J. Paradziej-Lukowicz, S. Martelli and J. Konopa, *J. Med. Chem.*, 1996, **39**(5), 1028–1032.
28 N. Martin, M. Quinteiro and C. Seoane, *Heterocycl. Chem.*, 1995, **32**(1), 235–238.
29 X.-S. Wang, D.-Q. Shi, Y.-F. Zhang, S.-H. Wang and S.-J. Tu, *Chin. J. Org. Chem.*, 2004, **24**(4), 430–432.
30 T.-S. Jin, J.-S. Zhang, T.-T. Guo, A.-Q. Wang and T.-S. Li, *Synthesis*, 2004, **2004**(12), 2001–2005.
31 K. Venkatesan, S. S. Pujari and K. V. Srinivasan, *Synth. Commun.*, 2009, **39**(2), 228–241.
32 B. Das, P. Thirupathi, I. Mahender, V. S. Reddy and Y. K. Rao, *J. Mol. Catal. A: Chem.*, 2006, **247**(1–2), 233–239.
33 S. Balalaie, F. Chadegani, F. Darviche and H. R. Bijanzadeh, *Chin. J. Chem.*, 2009, **27**(10), 1953–1956.
34 S.-J. Tu, C.-B. Miao, Y. Gao, Y.-J. Feng and J.-C. Feng, *Chin. J. Chem.*, 2002, **20**(7), 703–706.
35 X.-S. Wang, D.-Q. Shi, S.-H. Wang and S.-J. Tu, *Chin. J. Org. Chem.*, 2003, **23**(11), 1291–1293.
36 Z.-Q. Tang, Y. Chen, C.-N. Liu, K.-Y. Cai and S.-J. Tu, *Heterocycl. Chem.*, 2010, **47**(2), 363–367.
37 G. M. Ziarani, A. Badiei, M. Hassanzadeh and S. Mousavi, *Arabian J. Chem.*, 2021, **47**, 2845–2855.
38 M. Khalil, G. T. M. Kadja and M. M. Ilmi, *J. Ind. Eng. Chem.*, 2021, **93**, 78–100.
39 V. Polshettiwar, D. Cha, X. Zhang and J. M. Basset, *Angew. Chem., Int. Ed.*, 2010, **49**, 9652.
40 A. Maity and V. Polshettiwar, *ChemSusChem*, 2017, **10**, 3866.
41 H. Navay Baghban, M. Hasanzadeh, Y. Liu and F. Seidi, *Biosensors*, 2022, **12**(10), 911–925.
42 M. Baghal Behyar, F. Farshchi and M. Hasanzadeh, *J. Mol. Recognit.*, 2022, **35**(8), e2960.
43 **https://en.wikipedia.org/wiki/Hexamethylenetetramine**.
44 R. Ghorbani-Vaghei and V. Izadkhah, *Appl. Organomet. Chem.*, 2018, **32**, e4025.
45 S. Noori, R. Ghorbani-Vaghei and M. Mirzaei-Mosbat, *J. Mol. Struct.*, 2020, **1219**, 128583.
46 M. Mahmudi, N. Shadjou and M. Hasanzadeh, *J. Electroanal. Chem.*, 2019, **848**, 113272.
47 B. Karami, Sh. Nejati and Kh. Eskandari, *Curr. Chem. Lett.*, 2015, **4**, 169.
48 B. Mombaini, A. Kiasat and A. Ezabadi, *Orient. J. Chem.*, 2015, **31**, 483.
49 S. K. Kantevari, R. Bantu and L. J. Nagarapu, *J. Mol. Catal. A: Chem.*, 2007, **269**, 53.
50 A. Zare, A. R. Moosavi-Zare, M. Merajoddin, M. A. Zolfigol, T. Hekmat-Zadeh, A. Hasaninejad, A. Khazaei, M. Mokhlesi, V. Khakyzadeh, F. Derakhshan-Panah, M. H. Beyzavi, E. Rostami, A. Arghoon and R. Roohandeh, *J. Mol. Liq.*, 2012, **167**, 69.
51 M. M. Heravi, H. Alinejhad, Kh. Bakhtiari, M. Saeedi, H. A. Oskooie and F. F. Bamoharram, *Bull. Chem. Soc. Ethiop.*, 2011, **25**, 399.
52 F. Ghoreyshi Kahangi, M. Mehrdad, M. M. Heravi and S. Sadjadi, *Sci. Rep.*, 2020, **10**, 15285.
53 S. Rezayati, R. Hajinasiri, Z. Erfani, S. Rezayati and S. Afsharisharifabad, *Iran. J. Catal.*, 2014, **4**, 157.
54 G. R. Chaudhary, P. Bansal, N. Kaur and S. Mehta, *RSC Adv.*, 2014, **4**, 16377.
55 M. Hasanpour Galehban, B. Zeynizadeh and H. Mousavi, *J. Mol. Struct.*, 2023, **1271**, 134017.
56 S. E. Sadati Sorkhi, M. M. Hashemi and A. Ezabadi, *Res. Chem. Intermed.*, 2020, **46**, 2229.
57 M. Salami and A. Ezabadi, *Res. Chem. Intermed.*, 2020, **46**, 4611.
58 S. F. Hojati, M. Moosavifar and N. Moeinieghbali, *J. Chem. Sci.*, 2020, **132**, 38.
59 T. Josephrajan, V. T. Ramakrishnan, G. Kathiravan and J. Muthumary, *ARKIVOC*, 2005, **xi**, 124.
60 M. Bakherad, A. Keivanloo, A. H. Amin and A. Farkhondeh, *J. Mex. Chem. Soc.*, 2019, **63**, e2594.
61 N. Srividya, P. Ramamurthy, P. Shanmugasundaram and V. T. Ramakrishnan, *J. Org. Chem.*, 1996, **61**, 5083.
62 A. G. Swarna, A. S. Julie and J. A. Graham, *J. Med. Chem.*, 1999, **42**, 2383.
63 H. H. Lee and W. R. William, *J. Med. Chem.*, 1996, **39**, 2508.
64 (*a*) T. Eicher and S. Hauptmann, *The Chemistry of Heterocycles*, Wiley-VCH, 2003; (*b*) G. M. Ziarani, A. Badiei, M. Hassanzadeh and S. Mousavi, *Arabian J. Chem.*, 2014, **7**, 335339.
65 M. Kaya, Y. Yıldırır and G. Y. Celik, *Med. Chem. Res.*, 2011, **20**, 293.
66 M. Mazloumi and F. Shirini, *J. Mol. Struct.*, 2022, **1217**, 128326.
67 Z. Cui, L. Zhang, C. Chen and Y. Jiang, *Bioorg. Med. Chem.*, 2015, **24**, 261.
68 N. Hasannezhad and N. Shadjou, *J. Mol. Recognit.*, 2022, **35**, 2956.